



## Supramolecular Approach for Efficient Processing of Polylactide/Starch Nanocomposites

Samira Benali,<sup>\*,†</sup> Farid Khelifa,<sup>†</sup> Djahida Lerari,<sup>‡</sup> Rosica Mincheva,<sup>†</sup> Youssef Habibi,<sup>§</sup> Driss Lahem,<sup>||</sup> Marc Debliquy,<sup>||</sup> and Philippe Dubois<sup>†</sup>

<sup>†</sup>Center of Innovation and Research in Materials and Polymers (CIRMAP), Research Institute for Materials Science and Engineering, University of Mons (UMONS), Place du Parc 20, B-7000 Mons, Belgium

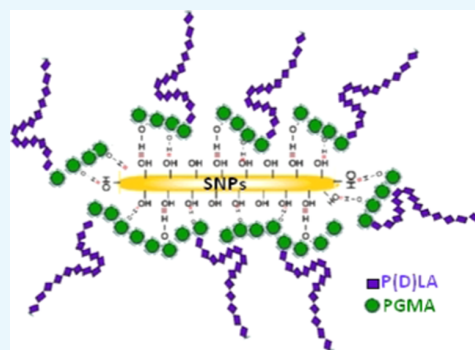
<sup>‡</sup>Centre de recherche scientifique et technique en analyses physico-chimiques, BP 384, CP 42004 Bou-Ismaïl, Tipaza, Algérie

<sup>§</sup>Materials Research and Technology (MRT), Luxembourg Institute of Science and Technology (LIST), Belval Innovation Campus, 5, avenue des Hauts-Fourneaux, L-4362 Esch-sur-Alzette, Luxembourg

<sup>||</sup>Service de Science des Matériaux, Faculté Polytechnique de Mons, Université de Mons, Rue de l'Épargne 56, B-7000 Mons, Belgium

### S Supporting Information

**ABSTRACT:** All-biobased and biodegradable nanocomposites consisting of poly(L-lactide) (PLLA) and starch nanoplatelets (SNPs) were prepared via a new strategy involving supramolecular chemistry, i.e., stereocomplexation and hydrogen-bonding interactions. For this purpose, a poly(D-lactide)-*b*-poly(glycidyl methacrylate) block copolymer (PDLA-*b*-PGMA) was first synthesized via the combination of ring-opening polymerization and atom-transfer radical polymerization. NMR spectroscopy and size-exclusion chromatography analysis confirmed a complete control over the copolymer synthesis. The SNPs were then mixed up with the copolymer for producing a PDLA-*b*-PGMA/SNPs masterbatch. The masterbatch was processed by solvent casting for which a particular attention was given to the solvent selection to preserve SNPs morphology as evidenced by transmission electron microscopy. Near-infrared spectroscopy was used to highlight the copolymer–SNPs supramolecular interactions mostly via hydrogen bonding. The prepared masterbatch was melt-blended with virgin PLLA and then thin films of PLLA/PDLA-*b*-PGMA/SNPs nanocomposites (ca. 600 μm) were melt-processed by compression molding. The resulting nanocomposite films were deeply characterized by thermogravimetric analysis and differential scanning calorimetry. Our findings suggest that supramolecular interactions based on stereocomplexation between the PLLA matrix and the PDLA block of the copolymer had a synergetic effect allowing the preservation of SNPs nanoplatelets and their morphology during melt processing. Quartz crystal microbalance and dynamic mechanical thermal analysis suggested a promising potential of the stereocomplex supramolecular approach in tuning PLLA/SNPs water vapor uptake and mechanical properties together with avoiding PLLA/SNPs degradation during melt processing.



## INTRODUCTION

Owing to their biobased nature and biodegradability, poly(L-lactide) (PLLA)-based packagings are promising for reducing the environmental impact of plastic materials.<sup>1</sup> Indeed, PLLA biodegradability is induced by hydrolysis of the ester bonds, leading to successive reductions of molecular weight, allowing the soil microorganisms to digest the oligomer fragments and reform CO<sub>2</sub>, H<sub>2</sub>O, and biomass as end products.<sup>2</sup> Furthermore, PLLA is a good candidate for new developments because of its physical and mechanical properties that can be tailored through polymer architecturing, allowing a good processability with the most commonly used industrial methods.<sup>1,3</sup>

When considering food packaging applications, the preparation of materials with interesting properties (mechanical, barrier, biodegradability, etc.) and guaranteeing complete food safety remain a real challenge. Among the strategies

investigated, the incorporation of nanoparticles seems most advantageous due to the large panel of fillers developed and available today.<sup>1,4–6</sup> Besides, particles can also impart to polymer matrices' enhanced mechanical and thermal performances as well as protection against gases, invasion of bacteria and microorganisms, harmful for food preservation.<sup>6</sup> In this context, the use of organomodified montmorillonite (clay) has already proved efficient.<sup>7</sup> Properties enhancement of clay-based nanocomposites results mainly from synergetic interactions between the high surface area of clay and the polymer chains.<sup>8</sup> Regarding more specifically PLLA, some interesting results have been obtained with a commercial organomodified clay, the

**Received:** October 1, 2017

**Accepted:** December 27, 2017

**Published:** January 26, 2018

Cloisite30B (CL30B). These PLLA/clay nanocomposites prepared by conventional melt extrusion exhibited remarkable oxygen permeability values, twice lower for hybrid systems with loadings up to 10 wt % of nanofillers compared to neat PLLA.<sup>9</sup> Recently, a PLLA/CL30B (3 wt %) nanocomposite substrate obtained by melt-mixing and coated with a thin plasma polymer film of ethyl lactate has demonstrated enhanced mechanical and optical properties as well as barrier properties with an oxygen transmission rate reduced by 53% with respect to neat PLLA, as reported by Ligot et al.<sup>10</sup> Even though these improvements are not sufficient for packaging applications, the use of nanoclays may find interest in the multilayer concept or can afford a control over the biodegradation of the material.<sup>11,12</sup> However, the toxicity effect of CL30B for food contact applications has been recently highlighted through *in vitro* experiments.<sup>13,14</sup> Moreover, CL30B also induced a statistical change of the ribonucleic acid messenger expression of the DNA. Nowadays, a specific genotoxicity evaluation, assessed by the European Food Safety Authority (EFSA), is still required for new substances intended to be used as food contact materials.<sup>14</sup> Thus, the development of new biobased and biodegradable nanofillers, responding also to environmental concerns, is highly encouraged.

With this respect, crystalline polysaccharide nanoparticles from renewable and biodegradable raw materials have drawn considerable attention of the scientific community. Among all, starch nanoparticles (SNPs) offer lots of promising opportunities in applications including drug delivery, nanoencapsulation, or in conferring additional properties to polymer matrices.<sup>15,16</sup> More importantly, an interesting aspect ratio with a platelet-like morphology makes them ideal candidates for barrier properties improvement of polymers.<sup>17</sup> Here, important challenges are the production and stabilization of the SNPs, as well as their dispersion/compatibilization in polymer matrices. Indeed, SNPs are mainly obtained via the dissolution and degradation of the amorphous domains in semicrystalline starch granules using acidic hydrolysis. Obviously, hydrolysis efficiency of starch granules depends on parameters such as temperature, acid nature, concentration, and botanic origin of the native starch, and is hard to handle with a limited/lack of control and morphology preservation.<sup>18</sup> Numerous other methods are reported for overcoming these issues, including extrusion,<sup>19,20</sup> high-pressure homogenization and emulsification,<sup>21,22</sup> ionic liquid medium,<sup>23,24</sup> solvent displacement method,<sup>18,25,26</sup> or ultrasonication,<sup>27</sup> with promising results for industrial applications.<sup>18</sup>

Surprisingly, even if SNPs seem to be highly appropriated for food packaging applications, the investigations in composite materials based on them are relatively scarce and only few matrices, including poly(styrene-*co*-butyl acrylate), natural rubber, pullulan, thermoplastic starch, poly(vinyl alcohol), soy protein, and waterborne polyurethane,<sup>18</sup> have been reported. The main issues preventing their use in a wider range of polymers are their lack of compatibility with many solvents usually employed in polymer solvent casting and their low thermal stability detrimental for melt-mixing processes.<sup>17,18,28</sup> To overcome these drawbacks and to possibly open a way for SNPs' industrial applications in composites, one of the strategies consists in surface modifications of nanoplatelets. Interestingly, starch nanocrystals are characterized by a reactive surface due to higher amount of hydroxyl groups available for further chemical modifications, and three main strategies have been reported so far: (i) chemical modification with small

molecules, (ii) "grafting onto" polymer chains with coupling agents, and (iii) "grafting from" polymer chains with polymerization of a monomer.<sup>28,29</sup>

In this study, PLLA/SNP composites have been prepared by melt-mixing process to produce films suitable for industrial applications. For this, two necessary prerequisites for a successful SNP incorporation, at PLLA processing temperature, have to be fulfilled. The first challenge consists in preserving the integrity of these SNPs highly sensitive toward temperature and solvents, and the second consists in achieving good dispersion and compatibility of particles with the matrix. A new strategy for the preparation of PLLA/SNP nanocomposites using a new compatibilizing diblock copolymer has been investigated. The copolymer is composed of (i) a poly(D-lactide) (PDLA) building block coined as *sc*-PLLA and (ii) a poly(glycidyl methacrylate) (PGMA) block. The as-synthesized PDLA-*b*-(PGMA)- coined as COPO- block copolymer was mixed up with SNPs by solvent casting and subsequently the resulting "masterbatch" was melt-processed with a commercially available poly(L-lactide) (PLLA) for forming a 600  $\mu\text{m}$  thick film by compression molding at 190 °C. For the sake of comparison, PLLA, PLLA/PDLA-*b*-PGMA, and PLLA/SNP samples were also prepared under the same experimental conditions. The potential of SNPs/COPO toward improving the water uptake and mechanical properties of poly(lactic acid) (PLA) was studied by quartz crystal microbalance (QCM) and dynamical mechanical analysis, respectively.

## RESULTS AND DISCUSSION

The original strategy proposed here for the preparation of PLLA/SNP nanocomposites with enhanced properties relies upon the use of a new compatibilizing diblock copolymer containing (i) a PDLA building block able to form thermostable PDLA-PLLA stereocomplexes at melt-processing temperature of the PLLA matrix,<sup>32,33</sup> i.e., 190 °C, and (ii) a poly(glycidyl methacrylate) block<sup>34–36</sup> with epoxy functional groups, which can interact with the hydroxyl groups available on SNP surfaces. The concept is illustrated in Figure 1.

**Synthesis of the P(D)LA-*b*-PGMA Copolymer.** To ensure good dispersion of the SNPs throughout the PLLA matrix, PGMA-*b*-P(D)LA diblock copolymers were purposely designed. The PGMA epoxy moieties are expected to interact through chemical and/or supramolecular grafting with the surface OH groups available on SNPs and consequently ensure

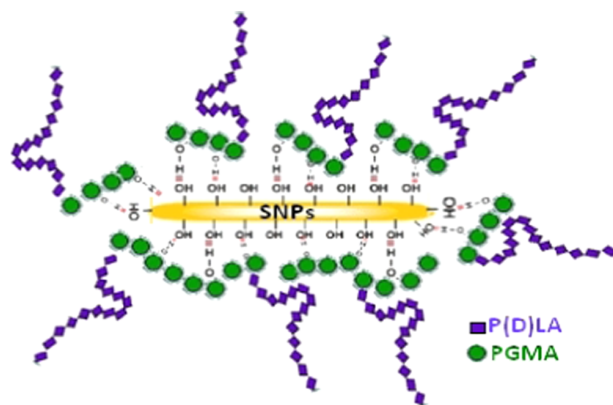


**Figure 1.** Schematic hydrogen-bonding interaction between P(D)LA-*b*-PGMA copolymers and SNP surface.

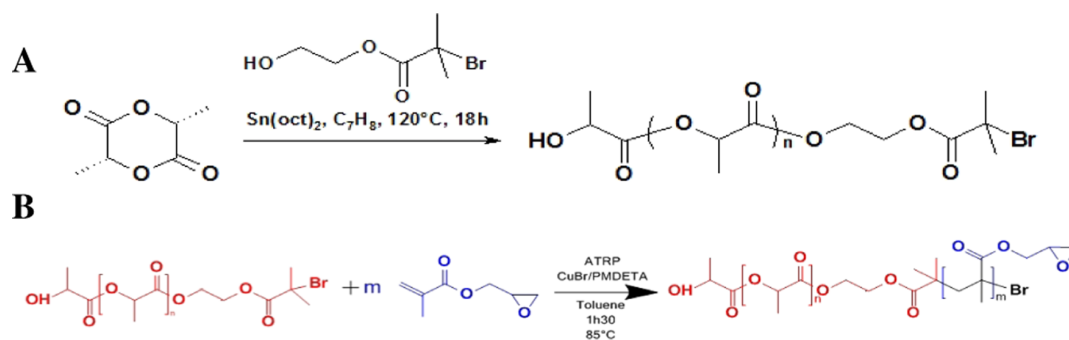


Figure 2. (A) P(D)LA macroinitiator synthesis. (B) P(D)LA-*b*-PGMA copolymer synthesis.

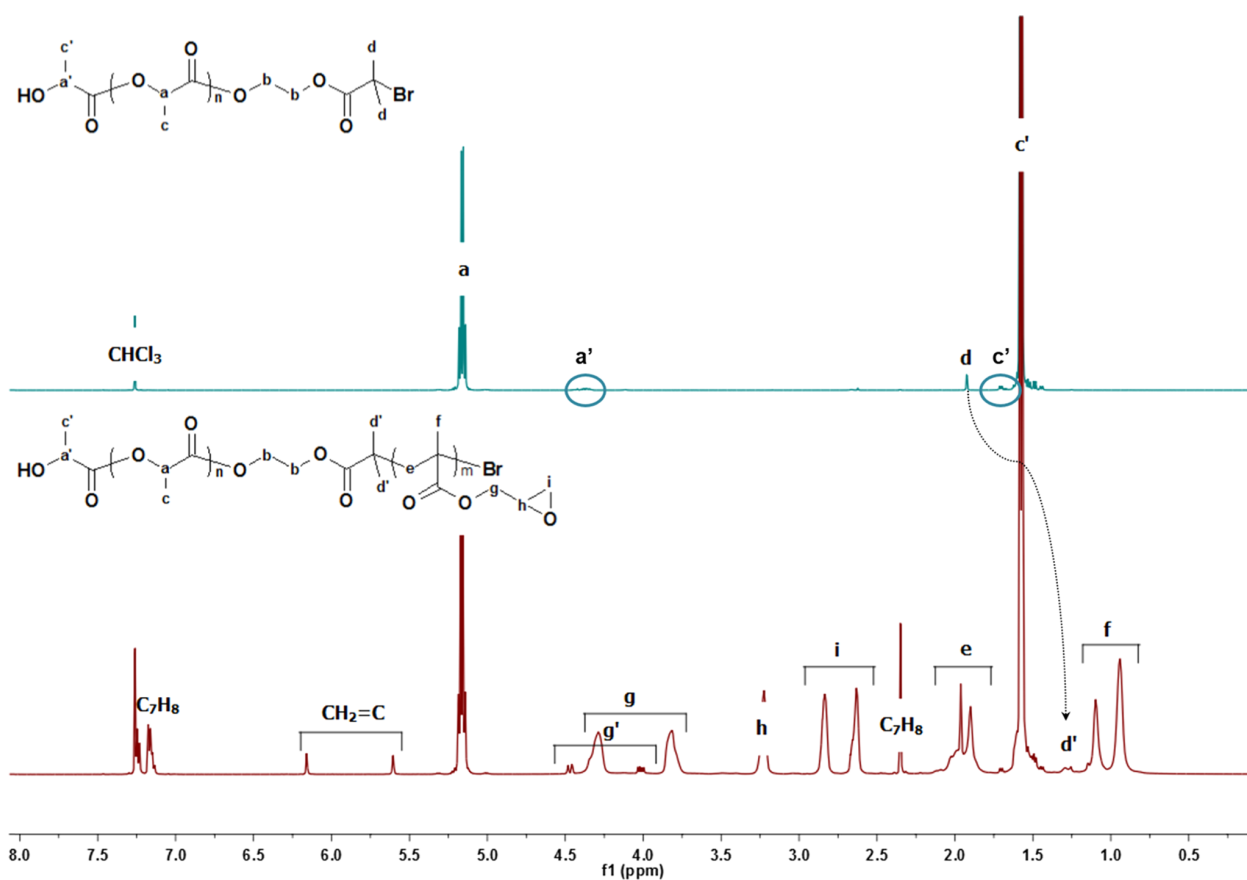


Figure 3.  $^1\text{H}$  NMR spectra of (top) P(D)LA-purified product and (bottom) P(D)LA-*b*-PGMA crude product in  $\text{CDCl}_3$ . The black arrow shows the shift of d protons after GMA polymerization. The PDLA-*b*-PGMA-purified spectra are available in the Supporting Information.

dispersibility (within the PLLA matrix) and thermal protection (during melt processing) of the grafted SNPs via supramolecular hydrogen bond-induced stereocomplexation between PDLA blocks and PLLA matrix.

The synthesis is based on the work published by Wolf et al., in which a poly(lactide)-*block*-poly(2-hydroxyethyl methacrylate) was reported.<sup>37</sup> It relies on a two-step process, including (i) the synthesis of a  $\alpha$ -hydroxy- $\omega$ -Br PDLA via lactide ring-opening polymerization (ROP) (Figure 2A), (ii) followed by PDLA-initiated atom-transfer radical polymerization (ATRP) of glycidyl methacrylate (GMA) (Figure 2B). The chemical structure of each block was confirmed by  $^1\text{H}$  NMR spectroscopy performed in deuterated chloroform as solvent (Figure 3). As expected, the PDLA spectrum presented all chemical signals

of the CH and the  $\text{CH}_3$  protons from the lactide monomer units. The chemical signal at 1.86 ppm was ascribed to the protons of the bromobutyryl  $\text{CH}_3$  groups (protons d, Figure 3, blue line). Furthermore, no residual lactide monomer could be observed after purification (Figure 3). In agreement with the expected PDLA-initiated ATRP of GMA, a clear shift of these protons to 1.22 ppm (protons d', Figure 3, black line) was observed in the NMR spectrum of the obtained copolymer, accompanied by the presence of the signals characteristic for the PGMA block. Thus, successful GMA polymerization is suggested. According to the literature,<sup>38</sup> the satellite signals denoted as "g" are ascribed to the  $\text{CH}_2$  groups next to the oxirane ring of the GMA monomer. Additionally, the chemical signals for the residual  $\text{CH}_2$  protons of the GMA double bond

**Table 1. Molecular Weights and Composition Data for P(D)LA Macroinitiators and the Resulting P(D)LA-*b*-PGMA Copolymer**

polymer	yield (%)	conversion (%)	$M_{n(\text{P(D)LA})}$ (g mol <sup>-1</sup> )	$M_{n(\text{exp(P(D)LA)})}$ (g mol <sup>-1</sup> )	$M_{n(\text{exp(PGMA)})}$ (g mol <sup>-1</sup> )	$D^{\text{SEC}}$
P(D)LA	96	97 <sup>a</sup>	14 500 <sup>a</sup>	16 400 <sup>b</sup>		1.15
P(D)LA- <i>b</i> -PGMA	73	93 <sup>c</sup>	14 500 <sup>a</sup>	16 400 <sup>b</sup>	13 350 <sup>c</sup>	1.14

<sup>a</sup>From <sup>1</sup>H NMR of crude reaction. <sup>b</sup>From <sup>1</sup>H NMR of purified P(D)LA product. <sup>c</sup>From <sup>1</sup>H NMR of copolymer.

were used to calculate a monomer conversion of 93%. Thus, the degree of polymerization of the PGMA block was calculated to be 94, and the  $M_n$  was found to be 13 350 g mol<sup>-1</sup> (Table 1).

The shift of the polymer elution trace toward lower elution volumes from size exclusion chromatography (SEC) analysis has also confirmed successfulness of the ATRP reaction (Figure 4). The narrow distribution curve ( $D^{\text{SEC}} < 1.15$ ) suggests a

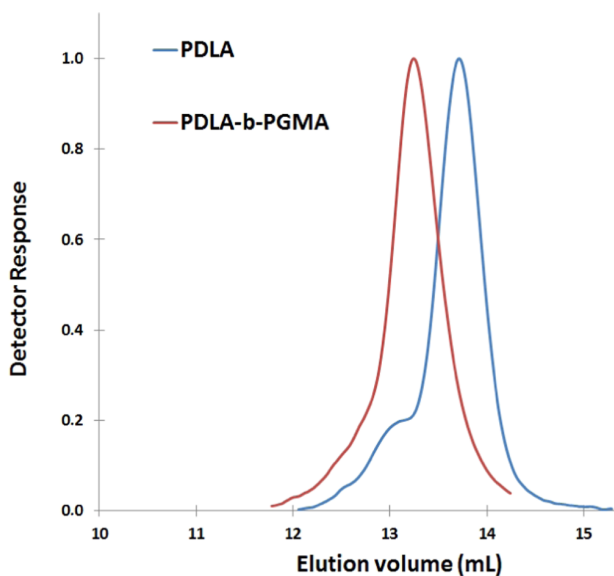


Figure 4. SEC images of P(D)LA and P(D)LA-*b*-PGMA copolymer.

good control over the copolymerization even though a small tail remains visible at lower elution volumes. This fraction of higher molecular mass copolymer chains likely results from the copolymerization reaction as initiated by some longer P(D)LA chains (also visible on the SEC trace of the macroinitiator and

probably formed by intermolecular transesterification reactions during the lactide ROP).

**Characterization of P(D)LA-*b*-PGMA Copolymer/SNPs Interactions.** To shed more light on the nature of the interactions between the PLLA, P(D)LA-*b*-PGMA copolymer, hereafter coined as COPO, and SNPs, near-infrared (NIR) spectroscopy was used. It is a useful technique for monitoring the possible etherification reaction between SNP hydroxyl and an epoxy ring<sup>39</sup> due to a strong absorption band, related to the oxirane group at 4534 cm<sup>-1</sup> that would decrease with epoxy ring opening by the OH function. Figure 5 depicts the NIR spectra obtained for COPO and COPO/SNP samples, with 50 wt % of SNPs, before and after drying step at 60 °C for 6 days. At 4534 cm<sup>-1</sup>, the spectrum of COPO is characterized by the C–H stretching and bending of epoxy ring with no modification before and after heat treatment. Similarly, for COPO/SNPs system, the characteristic band of epoxies is visible at 4540 cm<sup>-1</sup> both before and after heat treatment with same intensity, meaning that no reaction occurred. Therefore, the interactions between the epoxy rings and the SNP OH groups could not be easily identified. For a better understanding, a complete study must be realized and is currently in progress, but the main subject of this article is to highlight the interest of the PDLA-*b*-PGMA for melt processing of PLLA/SNP materials.

**PLLA/SNPs-Based Nanocomposites.** For comparison, as dimethyl formamide (DMF) is miscible in CHCl<sub>3</sub> and for promoting the drying step, the casting process of PLLA/SNP composites was conducted in a CHCl<sub>3</sub>/DMF mixture (8.7% of DMF). After an efficient drying step (see Experimental Part), thin films of PLLA/SNP nanocomposites were obtained using compression-molding techniques at 190 °C (Table 2).

**Visual Aspect and Transmission Electron Microscopy (TEM) Analyses.** Visual observations were used to appreciate the effect of the processing method on the film's aspect. Indeed, when thermally unstable SNPs are to be incorporated into a polymer matrix via high-temperature melt processing (at 190 °C for PLA), the expected coloration will be very indicative for

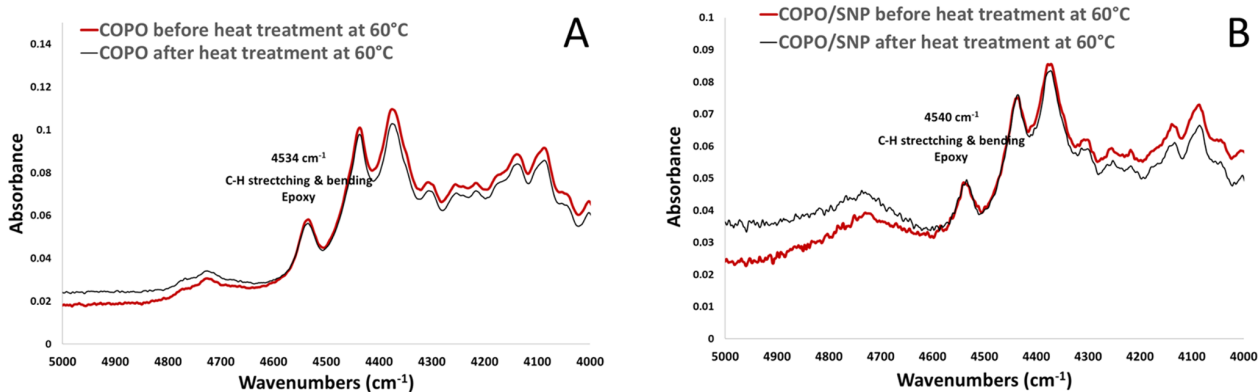


Figure 5. NIR spectra of COPO (A) and COPO/SNPs with 50 wt % of SNPs (B) before (line) and after (dash) heat treatment during 6 days at 60 °C.

**Table 2. Composition of PLLA, PLLA/COPO, PLLA/SNP, and PLLA/COPO/SNP Samples**

sample	content (wt %)
PLLA	100
PLLA/COPO	97/3
PLLA/SNPs	97/3
PLLA/COPO/SNPs	94/3/3

the composite thermal stability. Photos of the films after processing are presented in Figure 6, evidencing composition-dependent thermal stability. As expected, the PLLA sample is colorless and transparent, which is characteristic of the commercial-grade PLLA with low D-LA content and low crystallinity degree (see Experimental Part). The PLLA/SNP sample is rather brown, most probably due to an important degradation of the fillers and/or PLLA. In sharp contrast, the PLLA/COPO/SNPs remain colorless and transparent with no visible aggregates. To highlight the possible degradation, SEC measurements have been attempted but data were not acquired because of difficulty to selectively recover the PLLA chains fully deprived from the starch nanocrystals. Interestingly, differences in filtration were observed depending on samples. If PLLA filtration was very easy, then filtration of the PLLA/SNP sample was more difficult and totally impossible for the PLLA/COPO/SNP film, confirming further the strong supramolecular interactions between COPO epoxy groups and SNP hydroxyl groups.

It comes out that the incorporation of COPO allows certain compatibility between SNPs and PLLA matrix (PLLA/COPO/SNPs = 94/3/3 wt %) and provides a sufficient interfacial synergy between PLLA and SNPs for protecting SNPs from thermal decomposition.

Morphological investigations by TEM also revealed differences in SNP dispersion between PLLA/SNP and PLLA/COPO/SNP samples (Figure 7). Concerning PLLA/SNPs, only SNP aggregates or agglomerates are visible (see black dots), whereas PLLA/COPO/SNPs present very few small aggregates of around 200 nm diameter (black object). However, regardless of the samples, no individual SNPs could be clearly observed at both low and high magnifications probably due to charge effects and lack of contrast as a result of the organic nature of SNPs, COPO, and PLLA.

For focusing on possible effect of the finer dispersion of SNPs onto the PLLA/SNPs nanocomposite properties, thermal stability, crystallinity, and water adsorption were investigated

with thermogravimetric analysis (TGA), differential scanning calorimetry (DSC), and QCM analysis, respectively.

**Thermal Behavior.** Thermal degradation of PLLA, PLLA/COPO, PLLA/SNP, and PLLA/COPO/SNP nanocomposites was studied by thermogravimetric analysis (TGA) under nitrogen flow (Figure 8). The maximum in the first derivative thermogravimetry (DTG) was chosen to compare the thermal behavior of the nanocomposites. As expected, PLLA thermal degradation occurs in one step characterized by a maximum of DTG at 370 °C with no charred residue. With 3 wt % of COPO, the maximum of DTG remains constant (i.e., 374 °C).

In contrast, with 3 wt % SNPs, the maximum of DTG is largely shifted to lower temperatures (i.e., 348 °C). This result, showing a possible alteration of PLLA structure, confirms first conclusions drawn from the visual aspect of the PLLA/SNP film that appeared brown (Figure 6). The degradation phenomena observed by both analyses could be explained by a reaction, occurring during melt processing, of SNP hydroxyl groups on PLLA inducing polyester chain scission. PLLA degradation is well documented, and factors including temperature, pH, and presence of terminal carboxyl or hydroxyl groups are known to induce it.<sup>40</sup> Thus, these processes generally lead to a decrease of the molecular weight of PLLA, resulting in less thermally stable shorter chains.<sup>41</sup> Regarding PLLA/COPO/SNP sample, TGA analysis presents a maximum DTG at the same temperature as neat PLLA (i.e., 370 °C). Very interesting, and also in agreement with visual aspects, no effect of SNPs on PLLA integrity is noted on DTG curve. In this case, the preformed supramolecular hydrogen bonds between the epoxy groups of the compatibilizer and hydroxyl groups of SNPs likely prevent both the nanoplatelets and the PLLA matrix from degradation during melt processing.

A series of DSC experiments were then conducted for further investigating the thermal properties of PLLA/SNP nanocomposites (Figure 9). Thermograms are shifted vertically to facilitate interpretation. Data of DSC first heating cycle, such as cold crystallization temperature ( $T_{cc}$ ), melting point temperature ( $T_m$ ), endothermic cold crystallization, the corresponding enthalpies ( $\Delta H_{cc}$  and  $\Delta H_m$ ), stereocomplex melting temperature ( $T_{m(sc-PLA)}$ ), and stereocomplex melting enthalpy ( $\Delta H_{m(sc-PLA)}$ ), are summarized in Table 3. The neat PLLA matrix exhibits a semicrystalline behavior with a very broad cold crystallization, the peak temperature ( $T_c$ ) of which is at 113 °C, and endothermic melting occurring at a melting temperature ( $T_m$ ) of 168 °C. As expected, the DSC analysis of the

**Figure 6.** Visual aspects of PLLA, PLLA/SNP, and PLLA/COPO/SNP nanocomposite films as obtained by compression molding at 190 °C.

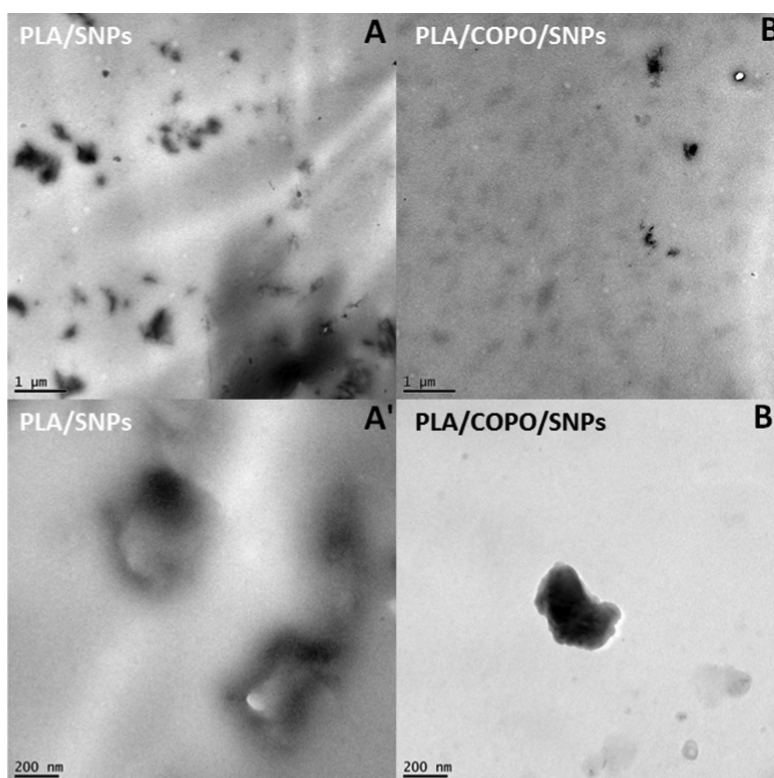


Figure 7. TEM images of PLLA/SNPs (A, A') and PLLA/COPO/SNPs (B, B').

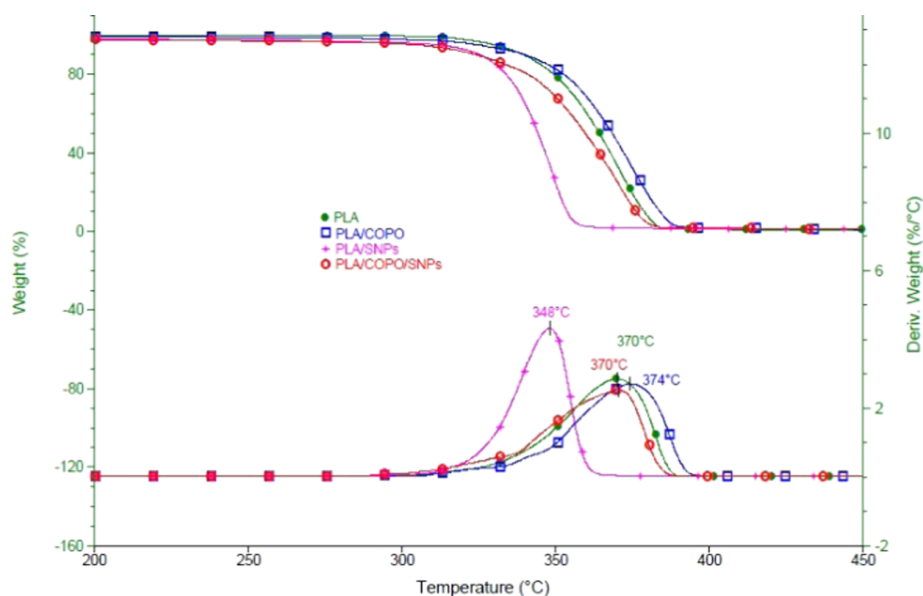
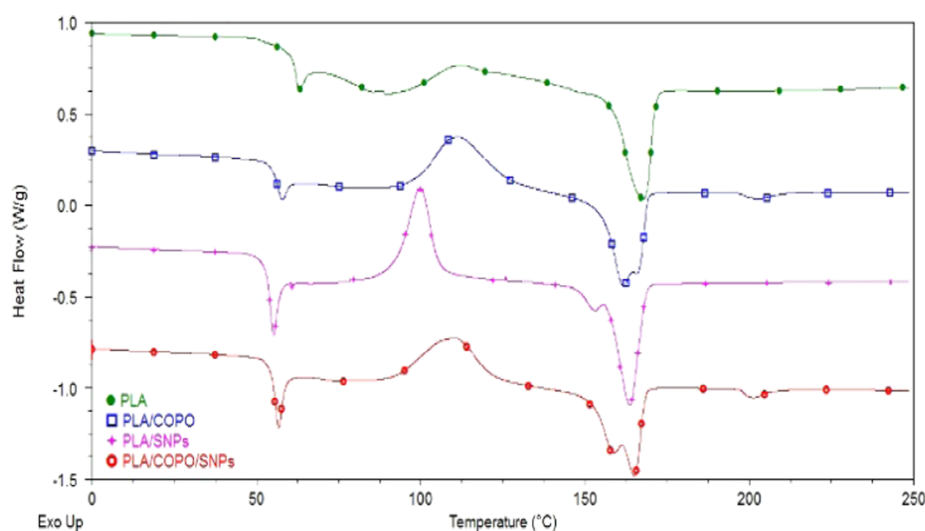


Figure 8. TGA analysis curves of PLLA (●), PLLA/COPO (□), PLLA/SNPs (\*), and PLLA/COPO/SNPs (○) with 3 wt % of SNPs under N<sub>2</sub>, at 20 °C min<sup>-1</sup>.

PLLA/COPO sample exhibits two endothermic melting peaks: the first one at 162 °C due to homo-PLLA crystallite and the second peak at 203 °C due to sc-PLLA.<sup>30</sup> Noteworthy, the PLLA melting endotherm (at 162 °C) turned bimodal due to melt recrystallization or the formation of  $\alpha'$ -PLA crystals generated during thermal treatment and coexisting with the regular  $\alpha$  form.<sup>7,42</sup> Besides, no significant influence of the presence of 3 wt % COPO was found on crystallinity because values of 3.0

and 3.7% have been calculated for samples PLLA and PLLA/COPO, respectively. This is in agreement with the literature,<sup>43</sup> demonstrating that for blends containing less than 6 wt % of PDLA, the crystallites are not fully developed upon cooling from the melt. Moreover, taking into account the PDLA weight content measured herein (1.5 wt %), the  $\Delta H_{m(sc)}$  value for the (PLLA/COPO) sample (i.e., 65 J g<sup>-1</sup><sub>sc-PLA</sub> recalculated considering 3 wt % of stereocomplex in the entire sample)



**Figure 9.** DSC analyses of PLLA (●), PLLA/COPO (□), PLLA/SNPs (\*), and PLLA/COPO/SNPs (○) with 3 wt % of SNPs. First heating at 10 °C min<sup>-1</sup>.

**Table 3.** DSC Results of PLLA–SNP-Based Nanocomposites<sup>a</sup>

	$T_{cc}(\text{homoPLLA})$ (°C)	$T_m(\text{homoPLLA})$ (°C)	$\Delta H_{cc}^b$ (J g <sup>-1</sup> <sub>homo-PLLA</sub> )	$\Delta H_m^b$ (J g <sup>-1</sup> <sub>homo-PLLA</sub> )	$\chi_c(\text{homoPLLA})$ (%)	$T_m(\text{sc-PLA})$ (°C)	$\Delta H_m^c$ (J g <sup>-1</sup> <sub>sc-PLA</sub> )
PLLA	113	168	29	31	3.0		
PLLA/COPO	111	162	33	37	3.7	203	65
PLLA/SNPs	102	164	32	38	7.1		
PLLA/COPO/SNPs	111	163	31	35	4.8	203	57

<sup>a</sup>10 °C min<sup>-1</sup>, first heating scan. <sup>b</sup> $\Delta H_m(\text{homo-PLLA})$  values recalculated according to PLLA subtracting the amount of PLLA supposed to participate in stereocomplexes formation (3 wt %). <sup>c</sup> $\Delta H_m(\text{sc-PLA})$  values recalculated according to 3 wt % of stereocomplexes (sc) possibly formed.

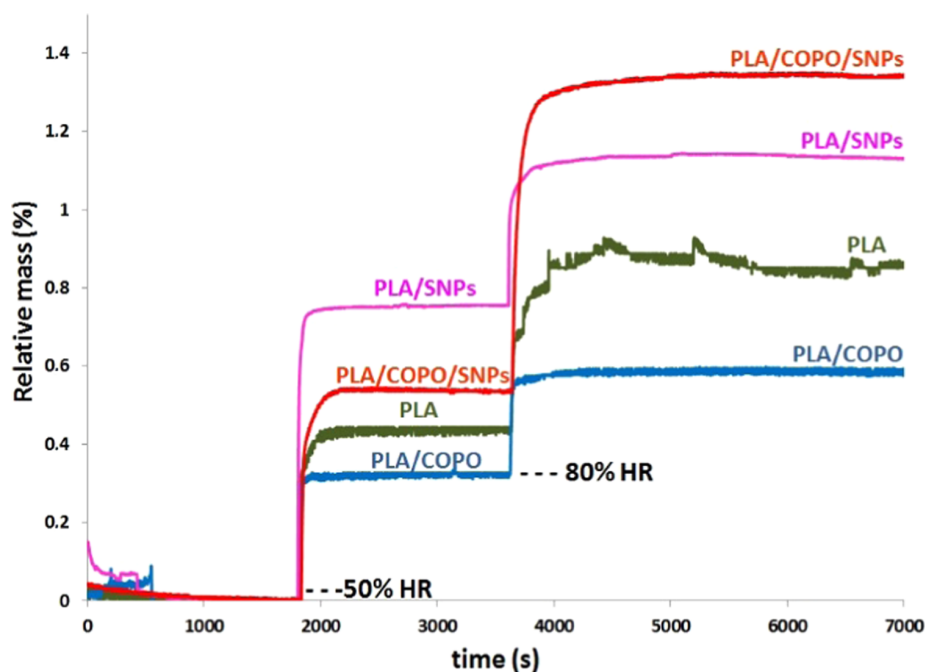


**Figure 10.** Time dependence of the relative mass change for thin PLLA/SNP-based films upon two relative humidity increase steps from 0 to 50% (after 1800 s) and then from 50 to 80% RH (after 3600 s). Legends are added above the corresponding curve at each step.

was lower than the value reported in the literature for the sc-PLA measured with pure stereocomplex (i.e.,  $\Delta H_m(\text{sc}) = 142 \text{ J g}^{-1}_{\text{sc-PLA}}$ <sup>32,44</sup>). One would assume that the mobility of PDLA for

initiating stereocomplexation is hindered by PGMA block. These results suggest that global PLLA crystallization degree is depressed by the procedure and more particularly by the rapid

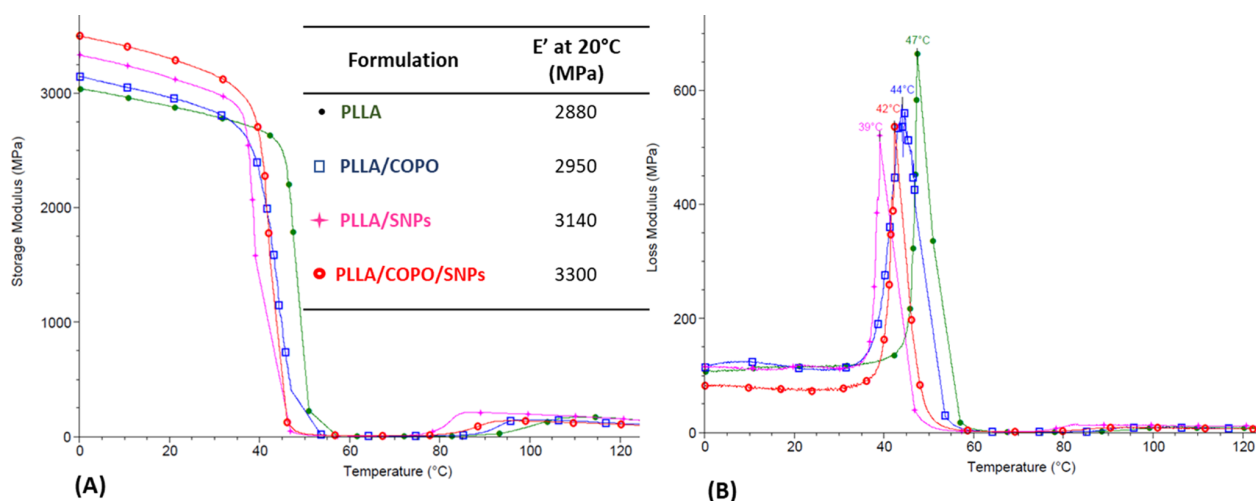


**Figure 11.** DMTA traces of (A) storage modulus ( $E'$ ) and (B) loss modulus ( $E''$ ) of PLLA (●), PLLA/COPO (□), PLLA/SNPs (\*), and PLLA/COPO/SNPs (○) with 3 wt % SNPs.

cooling of the samples to room temperature after melting, leading to a minimal nucleating effect of PLLA and a possible epitaxial crystallization of homocrystallites of PLLA on sc-PLA.<sup>30</sup>

Concerning the PLLA/SNP sample,  $T_{cc}$  of PLLA shifted toward lower temperatures (i.e.,  $T_{cc(\text{homoPLL})}$  (PLLA/SNPs) = 102 °C vs  $T_{cc(\text{homoPLL})}$  (PLLA) = 111 °C) confirming the assumption of PLLA degradation during melt processing. A 2-fold increase in PLLA crystallinity value (Table 3) was also observed, which may be due to shorter macromolecular chain lengths that induce more mobility promoting higher crystallization. Regarding the thermal properties of PLLA/COPO/SNPs, the  $T_{cc}$  of PLLA appears at the same temperature as neat PLLA and the corresponding crystallinity degree remains in the same range. However, the PLLA melting endotherm also became bimodal, highlighting the formation of crystals with different morphologies. The sc-PLA is always observed at 203 °C, and we can note that  $\Delta H_{m(\text{sc-PLA})(\text{PLLA/COPO/SNPs})}$  is slightly lower than  $\Delta H_{m(\text{sc-PLA})(\text{PLLA/COPO})}$ , i.e., 57 vs 65 J g<sup>-1</sup><sub>(sc-PLA)</sub>. To sum up, from all characterizations, it can be reasonably concluded that prior mixing of copolymer and SNPs leads to a good protection of SNPs from thermal degradation due to strong interactions between SNP hydroxyl groups and PGMA epoxy rings. Moreover, the selection of PDLA as the copolymer second block allowed the formation of PLLA/PDLA stereocomplexes, promoting further the good dispersion of SNPs into PLLA matrix.

#### QCM Analysis of PLLA/SNP-Based Nanocomposites.

Quartz crystal microbalance measurements on cast (nanocomposite)films were used to investigate the water sorption properties of the samples when exposed to humid environment.<sup>45</sup> For this, changes in frequency ( $\Delta f$ ) and thus in mass (cf. eq 2) were recorded as a function of relative humidity (RH), which successively increased from 0 to 50% (after 1800 s) and from 50 to 80% (after 3600 s). As noted in Experimental Part,  $\Delta f$  is initially taken as zero after overnight drying of samples on the QCM. Representative data are shown in Figure 10.

As seen, when samples are exposed to a 50% relative humidity (RH), relative mass uptakes of 0.41, 0.32, 0.73, and 0.54% were calculated for PLLA, PLLA/COPO, PLLA/SNPs, and PLLA/COPO/SNPs, respectively, stating that films filled

with SNPs (highly hydrophilic fillers) absorb generally more water than the polymer matrix. However, these preliminary results have to be carefully considered, knowing that part of the PLLA might be degraded during melt processing. Sharp et al.<sup>46</sup> found that the penetration of water in a PLLA homopolymer significantly depends on the polyester  $M_n$  due to plasticizing effect. By increasing the RH rate to 80%, one can still note higher water absorption for PLLA/SNPs in comparison to PLLA, i.e., 1.1% of RH against 0.86% of RH, respectively.

Regarding PLLA/COPO and PLLA/COPO/SNPs at 50% RH, two opposite effects were observed. Although the presence of 3% COPO within PLLA seems to increase the hydrophobicity of the blend material, the presence of SNPs increases its hygroscopic character. Thus, the PLLA/COPO/SNP composite film absorbs more water than PLLA/COPO but less water than PLLA/SNPs. Of course, the preservation of PLLA molar mass could also play a role and cannot be excluded. Similar results were obtained at 80% RH and might be explained with the plasticizing effect, impeding the decrease in the sorption rate over time.<sup>46</sup> It might be thus concluded that the optimization of water uptake for a specific application has to consider opposite composition-related and plasticizing effects.

#### Thermomechanical Properties of PLLA/SNP-Based Nanocomposites.

Dynamic mechanical thermal analysis (DMTA) can provide reliable information on the storage modulus ( $E'$ ), i.e., the elastic response to deformation (Figure 11A) and the loss modulus ( $E''$ ), i.e., the viscous response to deformation (Figure 11B) of (composite) polymeric materials. Data have shown that  $E'$  values of all melt-blended samples decrease gradually upon heating from 0 to 75 °C, with a more rapid decrease in the glass-transition region of PLLA, between 35 and 50 °C. Below the  $T_g$  (e.g., at 20 °C), native PLLA is characterized by a lowest storage modulus, whereas PLLA/COPO shows a slightly higher value, suggesting that the copolymer addition affects PLA chain mobility. The blend polymers remain stiffer, and the polymer flow is restricted. This effect can also be observed in the  $\alpha$ -transition region derived from the loss modulus curves (Figure 11A). The slight shift of  $E''$  from 47 to 44 °C indicates that the presence of the copolymer hinders the mobility of PLLA chains.

Adding SNPs to the neat PLLA matrix using melt blending leads to a material with a storage modulus higher than neat PLLA (+8%), highlighting the interest of starch nanoparticles for mechanical properties. However, the shift of the peak of loss modulus from 47 to 39 °C confirms that the presence of SNPs leads to a degradation of PLLA matrix and thus increases the mobility of the shorter chains of PLLA after glass transition. Regarding PLLA/COPO/SNPs, a highest storage modulus with an improvement of 12% compared to PLLA/COPO is observed. More interestingly, the loss modulus of PLLA/COPO/SNPs is similar to that of PLLA/COPO. Therefore, it might be considered that the use of copolymer PDLA-*b*-PGMA is a promising strategy for preparing all-biobased composites for food packaging.

## CONCLUSIONS

In this study, investigations on PLLA/SNP-based nanocomposites obtained by melt processing are reported. For this, a copolymer PDLA-*b*-PGMA aiming at promoting a good dispersibility of the platelet nanofillers into PLLA matrix as well as preserving their morphology is first synthesized. It is expected to react via (i) strong supramolecular interactions and/or grafting of the epoxy functions of PGMA moieties and the hydroxyl groups of SNPs and (ii) supramolecular hydrogen-bond-related stereocomplexation between PDLA block and PLLA matrix thermoresistant at PLLA melt temperature (i.e., 190 °C). It was evidenced that the good synergetic effect of the copolymer on both SNPs and PLLA allowed for an improvement of the thermal stability and mechanical properties of PLLA with SNPs due to an efficient protected effect of copolymer PDLA-*b*-PGMA. Preliminary results on water uptake tests by QCM and DMTA open new perspectives for tuning the water absorption properties of PLA/SNPs using adapted compatibilizers, which allow to prepare melt-processed PLA/SNP materials.

## EXPERIMENTAL PART

**Materials.** Poly(L-lactide) (PLLA-4032D, NatureWorks LLC, film-grade,  $M_n(PS) = 143\,000$ ,  $D = 2$ , according to supplier: D-isomer = 1.4%; relative viscosity = 3.94; residual monomer = 0.14%), waxy maize (Roquette, 99% of amylopectin), 2-hydroxyethyl 2-bromo-2-methylpropanoate (HBMP, Sigma-Aldrich), tin(II)-2-ethylhexanoate ( $\text{Sn}(\text{Oct})_2$ , Sigma-Aldrich), and  $N,N,N',N'',N'''$ -pentamethyldiethylenetriamine (PMDETA, Sigma-Aldrich) were used as received. SNP preparation and characterization have been described in the Supporting Information. D-Lactide (Purasorb D, Purac) was stocked in a glovebox prior to use. Glycidyl methacrylate (GMA, Sigma-Aldrich) was dried over anhydrous calcium hydride for 24 h at room temperature and purified by vacuum distillation at 60 °C prior to use. Copper(I) bromide (CuBr, Sigma-Aldrich) was purified by three consecutive washings with acetic acid and methanol and stocked under inert atmosphere prior to use. Sulfuric acid ( $\text{H}_2\text{SO}_4$ ), chloroform ( $\text{CHCl}_3$ ), toluene, dimethyl formamide (DMF), and heptane were of reagent grade supplied by VWR. Dry solvents were obtained using an MBraun solvent purification system under  $\text{N}_2$  flow.

**Synthesis of the First Block Poly(D-Lactide) (P(D)LA) Macroinitiator.** PDLA was synthesized by ring-opening polymerization of D-Lactide (D-LA) catalyzed by tin(II) octoate and initiated by 2-hydroxyethyl 2-bromo-2-methylpropanoate (HBMP). Dry toluene (40 mL, 2 mL  $\text{g}^{-1}$  of LA) was added to

D-LA (20.3 g, 144.1  $\text{g mol}^{-1}$ , 140 mmol) in a flame-dried two-necked round-bottom glass flask equipped with a magnetic stirring bar. Then, the toluene solution of  $\text{Sn}(\text{Oct})_2$  (2.4 mL;  $5.8 \times 10^{-2}$  M solution; 405.1  $\text{g mol}^{-1}$ ;  $1.39 \times 10^{-4}$  mol) was added to the reaction medium with a flame-dried syringe. The solution was heated at 120 °C using an oil bath, and polymerization was initiated after 2 min by injection of HBMP (291 mg, 0.2 mL;  $1.3 \times 10^{-4}$  mol) under nitrogen flow. The reaction was conducted for 18 h before being stopped by cooling to room temperature. The obtained product was dissolved in  $\text{CHCl}_3$ , and an aliquot of the sample for conversion analysis was harvested prior purification by precipitation in excess of cold methanol. Then, the polymer was recovered by filtration using Büchner system and dried under reduced pressure at 30 °C up to a constant weight. A white powder was recovered (19.5 g, 96%). The respective chemical signals are:  $^1\text{H NMR}$  ( $\text{CDCl}_3$ , 500 MHz)  $\delta$  ppm: 1.57 (d,  $\text{CH}(\text{CH}_3)$ , poly(lactide) chain); 1.59 (d,  $\text{CH}(\text{CH}_3)$  term. unit); 1.91 (s,  $\text{BrC}(\text{CH}_3)_2$ ); 4.38 (q,  $\text{CH}(\text{CH}_3)$  term. unit); and 5.15 (q,  $\text{CH}(\text{CH}_3)$ , poly(lactide) chain).

**Synthesis of the Second Block Poly(Glycidyl Methacrylate) (PGMA).** The second block of the copolymer was synthesized using ATRP route from PDLA macroinitiator. In a typical polymerization, 5 g of macroinitiator PDLA [MA] (5 g, 16 411  $\text{g mol}^{-1}$ ,  $3.45 \times 10^{-4}$  mol), CuBr [I] (49.4 mg, 143.4  $\text{g mol}^{-1}$ ,  $3.45 \times 10^{-4}$  mol), and PMDETA [L] (60 mg, 173.3  $\text{g mol}^{-1}$ ,  $3.45 \times 10^{-4}$  mol) were dried using three freeze–pump–thaw cycles in a flame-dried two-necked round flask with a magnetic stirring bar. Dry toluene (100 mL, 85 °C) was used as solvent, and the monomer GMA [M] was previously dried under  $\text{CaH}_2$  overnight. The freshly distilled GMA (4.7 mL (4.9 g); 142.1  $\text{g mol}^{-1}$ ,  $3.45 \times 10^{-2}$  mol) was added to a second flame-dried two-necked round flask with a magnetic stirring bar. The polymerization started when the first mixture was transferred to the second flask ( $\text{MA}[1]/\text{I}[1]/\text{L}[1]/\text{M}[100]$ ) using a dried-flame capillary. After 90 min, the medium was cooled to room temperature. An aliquot of crude product was used for the conversion calculation by  $^1\text{H NMR}$  spectroscopy (Figure 3). Then, the product was recovered after precipitation in 7 volumes of *n*-heptane, filtered, and dried under hood for 48 h and under reduced pressure at room temperature overnight. The copper was extracted using an alumina-Celite column as attested by a white powder coloration (7.3 g), and the resulting PDLA-*b*-PGMA copolymer (referred to as COPO in the following sections) was characterized by  $^1\text{H NMR}$  spectroscopy.  $^1\text{H NMR}$  ( $\text{CDCl}_3$ , 500 MHz)  $\delta$  ppm: 0.70–1.10 (m,  $\text{C}(\text{CH}_3)(\text{COOCH}_2\text{CH}_2\text{O}-\text{CH}_2)$ ); 1.29 (d,  $\text{HOCH}(\text{CH}_3)$ , poly(lactide) term. unit); 1.58 ( $\text{OCH}(\text{CH}_3)$ , poly(lactide) chain), 1.70–2.05 (m,  $-\text{CH}_2\text{C}(\text{CH}_3)(\text{COOCH}_2\text{CH}_2\text{OH})$ ); 3.23 (s,  $-\text{COOCH}_2\text{CH}_2\text{OH}$ ); 3.82–4.29 (s,  $-\text{COOCH}_2\text{CH}_2\text{OH}$ ); 4.03–4.46 (p,  $\text{HOCH}(\text{CH}_3)$ ; poly(lactide) term. unit); and 5.17 (q,  $\text{CH}(\text{CH}_3)$ ; poly(lactide) chain).

**Preparation of PLLA-Based Nanocomposites.** A solvent exchange of the SNP aqueous suspension from water to acetone and to DMF was carried out using successive redispersion and centrifugations for 10 min at 13 000 rpm. From the obtained suspension of SNPs/DMF (0.8 wt % SNPs), PLLA-based nanocomposites with 3 wt % SNPs were prepared. The weight ratio of [COPO]/[SNPs] was fixed at 25.8/100 g and mixed with PLLA in a  $\text{CHCl}_3$ /DMF mixture (8.7% of DMF). To obtain solid samples, all solutions were first dried under reduced pressure (room temperature, 1 h) and

then in a ventilated oven (60 °C, 1 week) until reaching a complete removal of solvents as assessed by TGA (not shown here). The collected samples were finally compression-molded into 600  $\mu\text{m}$  films for 5 min at 190 °C under a pressure of 150 bar using an Agila PE20 hydraulic press and then rapidly cooled to room temperature.

**Characterizations.**  $^1\text{H}$  NMR spectra were collected in  $\text{CDCl}_3$  solution on a Bruker AMX-500 NMR spectrometer. PLLA and PDLA-*b*-PGMA solutions were prepared in  $\text{CHCl}_3$  (2 mg  $\text{mL}^{-1}$ ), and molecular weight parameters ( $M_n$ ,  $M_w$ , and  $\bar{D}$ ) were determined by SEC at 30 °C using an Agilent liquid chromatograph equipped with an Agilent degasser, an isocratic HPLC pump (flow rate = 1 mL  $\text{min}^{-1}$ ), an Agilent autosampler (loop volume = 100  $\mu\text{L}$ ; solution concentration = 2 mg  $\text{mL}^{-1}$ ), an Agilent-DRI refractive index detector, and three columns: a PL gel 5  $\mu\text{m}$  guard column and two PL gel Mixed-B 5  $\mu\text{m}$  columns (linear columns for separation of  $M_{w(\text{PS})}$  ranging from 200 to 4  $\times 10^5$  g  $\text{mol}^{-1}$ ). Polystyrene standards were used for calibration. Near-infrared spectra were recorded in transmission mode with a Bruker Tensor 27 infrared spectrometer. NIR analyses were performed on thin films prepared by solvent casting from chloroform/DMF solution. Samples were scanned in the frequency range of 4000–5000  $\text{cm}^{-1}$  at a resolution of 4  $\text{cm}^{-1}$  and an accumulation of 32 scans before and after heat treatment at 60 °C. TEM images of SNP suspensions and PLLA/SNP nanocomposites were obtained from a CM100 microscope (Philips, Eindhoven, The Netherlands) at an accelerated voltage of 100 kV. Sections of 80 mm thick nanocomposites were prepared at  $-130$  °C using a Reichert-Jung Ultracut FC4E microtome equipped with a diamond knife. Thermogravimetric analyses (TGA) were performed at a heating rate of 20 °C  $\text{min}^{-1}$  from room temperature to 800 °C using a Hi-Res TGA Q5000 device from TA Instruments (Del, NY). Thermodegradation was determined on approximately 10 mg of samples with platinum sample pan in 25  $\text{cm}^3$   $\text{min}^{-1}$  of nitrogen flow. A DSC Q2000 from TA Instruments was used for DSC analyses in nitrogen atmosphere. Samples (weight: about 5–7 mg) were sealed in aluminum DSC pans and placed in the DSC cell. The DSC was calibrated with indium. The samples were heated from 0 to 250 °C at a heating rate of 10 °C  $\text{min}^{-1}$ . Relevant data were collected from the first heating scan to evaluate the role of the stereocomplex (sc) in PLLA crystallization. Enthalpy values were calculated according to homo-PLLA to sc-PLA ratio. The degree of crystallization ( $\chi_{\text{c}(\text{homo-PLLA})}$ ) was obtained using eq 1

$$\chi_{\text{c}(\text{homo-PLLA})} = \left[ \frac{\Delta H_{\text{m}(\text{homo-PLLA})} - \Delta H_{\text{c}(\text{homo-PLLA})}}{\Delta H_{\text{m}(\text{homo-PLLA})}^0 \times \left(1 - \frac{\% \text{ wt}_{\text{filler}}}{100}\right)} \right] \times 100 \quad (1)$$

where  $\Delta H_{\text{m}(\text{homo-PLLA})}$  and  $\Delta H_{\text{c}(\text{homo-PLLA})}$  are the melting and cold crystallization enthalpies, respectively, of PLLA test sample,  $\Delta H_{\text{m}(\text{homo-PLLA})}^0$  is the melting enthalpy of the 100% crystalline homo-PLLA (93.0 J  $\text{g}^{-1}$ ),<sup>30</sup> and %  $\text{wt}_{\text{filler}}$  is the weight percentage of filler.  $\Delta H_{\text{m}(\text{sc})}$  corresponding to the melting of PLLA–PDLA stereocomplexes has been calculated taking into account only the amount of formed stereocomplex (3 wt %). Quartz crystal microbalance (QCM) was performed with a Seiko EG&G model 917 Quartz Cristal Analyser (QCA 917). Quartz crystals were provided by Ametek (Princeton Applied Research). A gold deposit (0.2  $\text{cm}^2$ , thickness  $\sim 3000$  Å) was immobilized on the crystal through a sublayer of

titanium (thickness  $\sim 500$  Å). For analyses, compressed samples were first solubilized into  $\text{CHCl}_3$  ( $\sim 2.5\%$ ). Then, 6  $\mu\text{L}$  of the solution was deposited on the electrode and dried under reduced pressure at room temperature overnight. The frequency was finally measured automatically at regular intervals and controlled relative humidity (RH, i.e., 30 min at 0% RH, 30 min at 50% RH, 90 min at 80% RH). The relationship between frequency of the quartz crystal and absorbed water mass is given by eq 2 obtained from the Sauerbrey relation<sup>31</sup>

$$\Delta F = \frac{(2.3 \times 10^{-6} F_0^2 \Delta M)}{A} \quad (2)$$

where  $\Delta F$  (Hz) is the frequency variation induced by the mass variation  $\Delta M$  (g);  $A$  is the “active area” of the crystal; and  $F_0$  is the initial frequency of the crystal. The rates of sorption were obtained using Fick’s law of diffusion. Dynamical mechanical thermal analyses (DMTAs) were performed with a DMAQ800 from TA Instruments from 0 to 140 °C on compression-molded (0.6 mm thick and 5 mm wide) sheets of either unfilled PLLA or PLLA starch nanocomposites. Measurements were carried out in tensile mode at 1 Hz with a deformation of 10  $\mu\text{m}$ . The heating rate was 3 °C  $\text{min}^{-1}$ . DMTAs were performed 1 week after preparation and were realized on three specimens for each formulation to check the reproducibility.

## ■ ASSOCIATED CONTENT

### 📄 Supporting Information

The Supporting Information is available free of charge on the ACS Publications website at DOI: 10.1021/acsomega.7b01465.

Preparation and characterization of starch nanoplatelet solutions (PDF)

## ■ AUTHOR INFORMATION

### Corresponding Author

\*E-mail: samira.benali@umons.ac.be.

### ORCID

Samira Benali: 0000-0001-7144-3077

Youssef Habibi: 0000-0001-7023-5233

### Notes

The authors declare no competing financial interest.

## ■ ACKNOWLEDGMENTS

The financial support from Wallonia and the European Commission in the frame of the FEDER 2014–2020 program (LCFM-BIOMAT project) is gratefully acknowledged.

## ■ REFERENCES

- (1) Auras, R.; Harte, B.; Selke, S. An Overview of Poly(lactides) as Packaging Materials. *Macromol. Biosci.* **2004**, *4*, 835–864.
- (2) Maharana, T.; Mohanty, B.; Negi, Y. S. Melt–solid polycondensation of lactic acid and its biodegradability. *Prog. Polym. Sci.* **2009**, *34*, 99–124.
- (3) Stevens, E. S. *Green Plastics: An Introduction to the New Science of Biodegradable Plastics*; Princeton University Press: Princeton, 2002; pp 1–238.
- (4) Bradley, E. L.; Castle, L.; Chaudhry, Q. Applications of nanomaterials in food packaging with a consideration of opportunities for developing countries. *Trends Food Sci. Technol.* **2011**, *22*, 604–610.
- (5) Ray, S.; Quek, S. Y.; Easteal, A.; Chen, X. D. The Potential Use of Polymer-Clay Nanocomposites in Food Packaging. *Int. J. Food Eng.* **2006**, *2*, 13.

- (6) Azedero, H. M. C.; Mattoso, L. H. C.; McHugh, T. H. Nanocomposites in Food packaging - A Review. In *Advances in Diverse Industrial Applications of Nanocomposites*; Boreddy, R., Ed.; InTech: Rijeka, Croatia, 2011; pp 57–78.
- (7) Courgneau, C.; Domenek, S.; Lebossé, R.; Guinault, A.; Avérous, L.; Ducruet, V. Effect of crystallization on barrier properties of formulated polylactide. *Polym. Int.* **2012**, *61*, 180–189.
- (8) Alexandre, M.; Dubois, P. Polymer-layered silicate nanocomposites: preparation, properties and uses of a new class of materials. *Mater. Sci. Eng., R* **2000**, *28*, 1–63.
- (9) Sorrentino, A.; Gorrasi, G.; Vittoria, V. Permeability in Clay/Polyesters Nano-Biocomposites. *Environ. Silic. Nano-Biocompos.* **2012**, *237–264*.
- (10) Ligot, S.; Benali, S.; Ramy-Ratiarison, R.; Murariu, M.; Snyders, R.; Dubois, P. Mechanical, Optical and Barrier Properties of PLA-layered silicate nanocomposites coated with Organic Plasma Polymer Thin Films. *Mater. Sci. Eng. Adv. Res.* **2015**, *1*, 20–30.
- (11) Rhim, J.-W. W.; Park, H.-M. M.; Ha, C.-S. S. Bio-nanocomposites for food packaging applications. *Prog. Polym. Sci.* **2013**, *38*, 1629–1652.
- (12) Benali, S.; Aouadi, S.; Anne-Laure, D.; Murariu, I. M.; Dubois, P. Key-factors for tuning the hydrolytic degradation of polylactide/Zinc oxide nanocomposites. *Nanocomposites* **2015**, 51–60.
- (13) Maisanaba, S.; Puerto, M.; Pichardo, S.; Jordá, M.; Moreno, F. J.; Aucejo, S.; Jos, Á. In vitro toxicological assessment of clays for their use in food packaging applications. *Food Chem. Toxicol.* **2013**, *57*, 266–275.
- (14) Maisanaba, S.; Jordá-Beneyto, M.; Cameán, A. M.; Jos, Á. Effects of two organomodified clays intended to food contact materials on the genomic instability and gene expression of hepatoma cells. *Food Chem. Toxicol.* **2016**, *88*, 57–64.
- (15) LeCorre, D.; Vahanian, E.; Dufresne, A.; Bras, J. Enzymatic pretreatment for preparing starch nanocrystals. *Biomacromolecules* **2012**, *13*, 132–137.
- (16) Habibi, Y.; Benali, S.; Dubois, P. In Situ Polymerization of Bionanocomposites. In *Handbook of Green Materials*; World Scientific Pub. Co., 2014; pp 69–88.
- (17) Le Corre, D.; Bras, J.; Dufresne, A. Starch nanoparticles: a review. *Biomacromolecules* **2010**, *11*, 1139–1153.
- (18) Kim, H.-Y.; Park, S. S.; Lim, S.-T. Preparation, characterization and utilization of starch nanoparticles. *Colloids Surf., B* **2015**, *126*, 607–620.
- (19) Song, D.; Thio, Y. S.; Deng, Y. Starch nanoparticle formation via reactive extrusion and related mechanism study. *Carbohydr. Polym.* **2011**, *85*, 208–214.
- (20) Giezen, F. E.; Jongboom, O. J.; Feil, H.; Gotlieb, K. F.; Boersma, A. Biopolymer Nanoparticles. U.S. Patent US6,677,386 B12004.
- (21) Shi, A.-m.; Li, D.; Wang, L. J.; Li, B. Z.; Adhikari, B. Preparation of starch-based nanoparticles through high-pressure homogenization and miniemulsion cross-linking: Influence of various process parameters on particle size and stability. *Carbohydr. Polym.* **2011**, *1604–1610*.
- (22) Liu, D.; Wu, Q.; Chen, H.; Chang, P. R. Transitional properties of starch colloid with particle size reduction from micro- to nanometer. *J. Colloid Interface Sci.* **2009**, *339*, 117–124.
- (23) Xie, W.; Zhang, Y.; Liu, Y. Homogenous carboxymethylation of starch using 1-butyl-3-methylimidazolium chloride ionic liquid medium as a solvent. *Carbohydr. Polym.* **2011**, *85*, 792–797.
- (24) Wilpiszewska, K.; Spychaj, T. Ionic liquids: Media for starch dissolution, plasticization and modification. *Carbohydr. Polym.* **2011**, *86*, 424–428.
- (25) Hebeish, A.; El-Rafie, M. H.; EL-Sheikh, M. A.; El-Naggar, M. E. Ultra-Fine Characteristics of Starch Nanoparticles Prepared Using Native Starch With and Without Surfactant. *J. Inorg. Organomet. Polym. Mater.* **2014**, *24*, S15–S24.
- (26) Qin, Y.; Liu, C.; Jiang, S.; Xiong, L.; Sun, Q. Characterization of starch nanoparticles prepared by nanoprecipitation: Influence of amylose content and starch type. *Ind. Crops Prod.* **2016**, *87*, 182–190.
- (27) Haaj, S. B.; Magnin, A.; Pétrier, C.; Boufi, S. Starch nanoparticles formation via high power ultrasonication. *Carbohydr. Polym.* **2013**, *92*, 1625–1632.
- (28) Raquez, J. M.; Goffin, A.-L.; Duquesne, E.; Habibi, Y.; Dufresne, A.; Dubois, P. Novel Nanocomposites Reinforced with Polysaccharide (Starch) Nanocrystals: from Interfacial Ring-Opening Polymerization to Melt-Processing Implementation. In *Biobased Monomers, Polymers and Materials*; Smith, P. B., Gross, R. A., Eds.; American Chemical Society: Washington, DC, 2012; pp 257–268.
- (29) Lin, N.; Huang, J.; Chang, P. R.; Anderson, D. P.; Yu, J. Preparation, modification, and application of starch nanocrystals in nanomaterials: a review. *J. Nanomater.* **2011**, *2011*, No. 573687.
- (30) Tsuji, H. Poly (lactide) stereocomplexes: formation, structure, properties, degradation, and applications. *Macromol. Biosci.* **2005**, *5*, 569–597.
- (31) Moylan, C. R.; Best, M. E.; Ree, M. Solubility of Water in polyimides: Quartz Crystal Microbalance Measurements. *J. Polym. Sci., Part B: Polym. Phys.* **1991**, *29*, 87–92.
- (32) Mincheva, R.; Raquez, J. M.; Lison, V.; Duquesne, E.; Talon, O.; Dubois, P. Stereocomplexes from biosourced lactide/butylene succinate-based copolymers and their role as crystallization accelerating agent. *Macromol. Chem. Phys.* **2012**, *213*, 643–653.
- (33) Re, G. L.; Benali, S.; Habibi, Y.; Raquez, J. M.; Dubois, P. Stereocomplexed PLA nanocomposites: From in situ polymerization to materials properties. *Eur. Polym. J.* **2014**, *54*, 138–150.
- (34) Fortunati, E.; Puglia, D.; Kenny, J. M.; Minhaz-Ul Haque, M.; Pracella, M. Effect of ethylene-co-vinyl acetate-glycidylmethacrylate and cellulose microfibrils on the thermal, rheological and biodegradation properties of poly(lactic acid) based systems. *Polym. Degrad. Stab.* **2013**, *98*, 2742–2751.
- (35) Yang, W.; Dominici, F.; Fortunati, E.; Kenny, J. M.; Puglia, D. Melt free radical grafting of glycidyl methacrylate (GMA) onto fully biodegradable poly(lactic) acid films: effect of cellulose nanocrystals and a masterbatch process. *RSC Adv.* **2015**, *5*, 32350–32357.
- (36) Khelifa, F.; Habibi, Y.; Benard, F.; Dubois, P. Effect of cellulosic nanowhiskers on the performances of epoxidized acrylic copolymers. *J. Mater. Chem.* **2012**, *22*, 20520–20528.
- (37) Wolf, F. F.; Friedemann, N.; Frey, H. Poly(lactide)-block-poly(HEMA) Block Copolymers: An orthogonal one-pot combination of ROP and ATRP, using a bifunctional initiator. *Macromolecules* **2009**, *42*, 5622–5628.
- (38) Yoshida, E. Selective Controlled/Living Photoradical Polymerization of Glycidyl Methacrylate, Using a Nitroxide Mediator in the Presence of a Photosensitive Triarylsulfonium Salt. *Polymers* **2012**, *4*, 1580–1589.
- (39) Khelifa, F.; Habibi, Y.; Bonnaud, L.; Dubois, P. Epoxy Monomers Cured by High Cellulosic Nanocrystal Loading. *ACS Appl. Interfaces* **2016**, *8*, 10535–10544.
- (40) Nampoothiri, K. M.; Nair, N. R.; John, R. P. An overview of the recent developments in polylactide (PLA) research. *Bioresour. Technol.* **2010**, *101*, 8493–8501.
- (41) Park, K. I.; Xanthos, M. A study on the degradation of polylactic acid in the presence of phosphonium ionic liquids. *Polym. Degrad. Stab.* **2009**, *94*, 834–844.
- (42) Zhang, J.; Tashiro, K.; Domb, A. J.; Tsuji, H. Confirmation of Disorder  $\alpha$  Form of Poly(L-lactic acid) by the X-ray Fiber Pattern and Polarized IR/Raman Spectra Measured for Uniaxially-Oriented Samples. *Macromol. Symp.* **2006**, *242*, 274–278.
- (43) Schmidt, S. C.; Hillmyer, M. A. Polylactide Stereocomplex Crystallites as Nucleating Agents for Isotactic Polylactide. *J. Polym. Sci., Part B: Polym. Phys.* **2001**, *39*, 300–313.
- (44) Tsuji, H.; Horii, F.; Nakagawa, M.; Ikada, Y.; Odani, H.; Kitamaru, R. Stereocomplex Formation between Enantiomeric Poly(lactic acid)s. 7. Phase Structure of the Stereocomplex Crystallized from a Dilute Acetonitrile Solution As Studied by High-Resolution Solid-State  $^{13}\text{C}$  NMR Spectroscopy. *Macromolecules* **1992**, *25*, 4114–4118.
- (45) Schuttlefield, J. D.; Cox, D.; Grassian, V. H. An investigation of water uptake on clays minerals using ATR-FTIR spectroscopy coupled

with quartz crystal microbalance measurements. *J. Geophys. Res.* **2007**, *112*, No. D21303.

(46) Sharp, J. S.; Forrest, J. A.; Jones, R. A. L. Swelling of Poly(dl-lactide) and Polylactide-co-glycolide in Humid Environments. *Macromolecules* **2001**, *34*, 8752–8760.